Systematic graphical correction of the hypernetted chain theory for the one-component plasma

1982 J. Phys. A: Math. Gen. 15 1007

(http://iopscience.iop.org/0305-4470/15/3/035)

J. Phys. A: Math. Gen. **15** (1982) 1007–1028. Printed in Great Britain

Systematic graphical correction of the hypernetted chain theory for the one-component plasma

David MacGowan

Department of Natural Philosophy, University of Glasgow, Glasgow G12 8QQ, UK

Received 21 August 1981

Abstract. The Fourier transforms of the lowest two orders of bridge graphs in the Abe–Meeron expansion for the one-component plasma are evaluated numerically after using the Goursat–Feynman relations to reduce the dimensionality of the integrals involved. After inverse Fourier transformation, the results are used to form approximants for the complete set of bridge graphs. These are then incorporated into modified hypernetted chain (HNC) theories which are expected to be useful in the intermediate-coupling regime. The results of the modified HNC equations improve upon the usual HNC results in terms of virial-compressibility consistency and they suggest that the excess internal energies found by Monte Carlo simulation may not be very reliable in the intermediate-coupling regime.

1. Introduction

In recent years there has been great interest in the statistical mechanics of strongly coupled plasmas. Baus and Hansen (1980) have given an excellent review of this subject. The simplest model system, which has been studied extensively, is the classical one-component plasma (OCP). It consists of classical point ions embedded in a uniform neutralising background. The OCP represents a good approximation to the material in the interior of a white dwarf star and is also useful as a reference system (Galam and Hansen 1976) for perturbative treatments of more realistic plasmas, such as those formed in the later stages of inertial confinement implosions.

We consider an OCP in thermal equilibrium at temperature $T = (k_B\beta)^{-1}$ and with ion density ρ. The interaction energy between a pair of ions at separation r is $\phi(r) = (Ze)^2/r$. The conventional coupling constant for a strongly coupled OCP is

$$\Gamma = \beta(Ze)^2/a \tag{1}$$

where $a = (3/4\pi\rho)^{1/3}$ is the ion sphere radius. However, since the present work utilises the weak-coupling (nodal) expansion, reviewed recently by Deutsch *et al* (1981), it is more appropriate to work in terms of the alternative coupling constant

$$\Lambda = \beta(Ze)^2/\lambda_D \tag{2}$$

where $\lambda_D = [4\pi\rho\beta(Ze)^2]^{-1/2}$ is the weak-coupling screening length (the Debye length). Λ and Γ are related by

$$\Lambda = 3^{1/2}\Gamma^{3/2}. \tag{3}$$

0305-4470/82/031007+22$02.00

In keeping with the use of (2) rather than (1), it is natural to work in terms of the dimensionless length

$$\xi = r/\lambda_D \tag{4}$$

rather than the more frequently used

$$x = r/a. \tag{5}$$

Since the present calculations involve the weak-coupling expansion, results obtained from them cannot be expected to apply beyond the weak- to intermediate-coupling regime. They will therefore be relevant to inertial confinement plasmas ($\Lambda \lesssim 2$) but probably not to much more strongly coupled plasmas such as those in white dwarf stars.

The thermal equilibrium of the OCP has been simulated using Monte Carlo (MC) techniques of increasing precision (Brush *et al* 1966, Hansen 1973, Slattery *et al* 1980) and the MC results are generally regarded as exact within statistical uncertainty. There is nevertheless great interest in obtaining accurate theoretical results for the OCP, partly due to the computer time requirements of MC simulations for multi-component ionic systems. One of the most fruitful approaches to a theoretical description of the OCP has been through the fluid structure integral equations, the best known of which are the Born–Green–Yvon, Percus–Yevick and hypernetted chain (HNC) equations. It is clear from a comparison of the results of Hirt (1967) and of Springer *et al* (1973) with MC data that the HNC equation is by far the best of these, both in terms of existence and accuracy of solutions. Ng (1974) has given an extremely accurate set of solutions of the HNC equation for a very wide range of values of Γ.

The HNC approximation for the OCP may be represented by the equation

$$g(\xi) = \exp[-(\Lambda/\xi) + h(\xi) - c(\xi)] \tag{6}$$

together with the exact relations

$$h(\xi) = g(\xi) - 1 \tag{7}$$

$$\hat{h}(k) = \hat{c}(k) + (4\pi\Lambda)^{-1}\hat{h}(k)\hat{c}(k). \tag{8}$$

Here $g(\xi)$ is the radial distribution function, $c(\xi)$ is the direct correlation function and the Fourier transforms involved in the Ornstein–Zernike relation (8) are defined by

$$\hat{f}(k) = \frac{4\pi}{k}\int_0^\infty d\xi\, \xi \sin k\xi f(\xi).$$

Once the equations (6)–(8) have been solved for the structure functions $h(\xi)$ and $c(\xi)$, the thermodynamic functions are easily obtained from them. The excess internal energy per ion u^{ex} is given by

$$\beta u^{ex} = \tfrac{1}{2}\int_0^\infty d\xi\, \xi h(\xi) \tag{9a}$$

$$= \frac{1}{4\pi^2}\int_0^\infty dk\, \hat{h}(k). \tag{9b}$$

The thermal pressure (defined by the density derivative of the Helmholtz free energy) is given by

$$\beta p/\rho - 1 = \tfrac{1}{3}\beta u^{ex}. \tag{10}$$

Structure and thermodynamics are also related through the compressibility equation

$$\beta\left(\frac{\partial p}{\partial \rho}\right)_\beta = 1 - \Lambda^{-1}\int_0^\infty \mathrm{d}\xi\,\xi^2\left(c(\xi)+\frac{\Lambda}{\xi}\right). \tag{11}$$

The principal merit of the HNC results for the OCP is that, irrespective of the coupling strength, they yield rather accurate values of u^{ex} through (9) despite the inaccuracy of the HNC $g(\xi)$ at strong coupling. This can be attributed to the fact that the HNC approximation reproduces the exact zeroth and second moments of $h(\xi)$ and is therefore expected to give an accurate (-1)th moment to which u^{ex} is proportional. Nevertheless, MC results show the non-static part of βu^{ex} at strong coupling to be $O(\Gamma^{1/4})$ as opposed to $O(\Gamma^{1/2})$ from the HNC results (De Witt 1976). The latter point is not especially significant in the intermediate-coupling regime where a more important shortcoming of HNC theory is its lack of thermodynamic consistency: that is, the exact thermodynamic relation

$$\beta(\partial p/\partial\rho)_\beta = 1 + \tfrac{1}{3}\beta u^{ex} + \tfrac{1}{9}\Gamma(\mathrm{d}/\mathrm{d}\Gamma)(\beta u^{ex}) \tag{12}$$

is not satisfied when βu^{ex} is taken from (9) and $\beta(\partial p/\partial\rho)_\beta$ from (11). Thus, although the HNC approximation is the best of the usual integral equation theories for the OCP, it still leaves considerable scope for improvement.

The HNC approximation was originally derived from the Mayer graphical expansion where (6) results from the exact relation

$$g(r) = \exp(-\beta\phi(r) + h(r) - c(r) + b(r)) \tag{13}$$

upon neglecting the bridge graphs $b(r)$. Various attempts to improve it have involved replacing $b(r) = 0$ by a more realistic approximation. Ng (1974) used the empirical expression

$$b(x) = -0.6\Gamma\,\mathrm{erf}(0.024\Gamma)/x \tag{14}$$

and achieved considerably enhanced accuracy for $g(x)$ despite the fact that $b(x)$ is known to be finite at $x = 0$ and of short range, both of which properties are violated by (14). This suggests that, in a modified HNC scheme, $g(x)$ is insensitive to the long- and short-range behaviour of $b(x)$ and so may depend crucially on its behaviour at intermediate x. Equation (14) does, however, cause other problems such as a divergence in (11).

MacGowan (1981) used the semi-empirical approximation

$$b(x) = P\exp(-x^2) \tag{15}$$

which does not violate any of the known behaviour of $b(x)$ and where the parameter P was chosen so as to yield values consistent with the exact result (Jancovici 1977)

$$\frac{\mathrm{d}^2}{\mathrm{d}x^2}\left(\ln g(x) + \frac{\Gamma}{x}\right)\bigg|_{x=0} = -\tfrac{1}{2}\Gamma. \tag{16}$$

Again (15), with P determined by (16), caused a considerable improvement in $g(x)$ but the thermodynamic consistency was even poorer than in the HNC approximation.

Rosenfeld and Ashcroft (1979) combined the imposition of virial-compressibility consistency with the idea of the reference HNC equation (Lado 1973). In effect they set the OCP bridge graphs equal to the exact bridge graphs of a hard-sphere reference fluid whose packing fraction was adjusted to achieve thermodynamic consistency. Their results are of wide applicability and very accurate (and *a priori* self-consistent).

In the present paper, calculations of the lowest two orders of bridge graphs in the Abe–Meeron nodal expansion for the OCP are reported. The asymptotic behaviours of these graphs in the $k \to 0$ limit (Deutsch *et al* 1976) and the $r \to \infty$ limit (Lavaud 1977) have been considered previously. Deutsch *et al* (1979) have also obtained the exponential factor in the $r \to \infty$ decay of these graphs by analytic evaluation of the corresponding graphs for a one-dimensional OCP, arguing that this exponential factor is independent of dimension. Very recently, after the present work had been completed, Furutani *et al* (1981) published accurate numerical results for the third-order bridge graph in three dimensions. The slightly less accurate results given below are, however, adequate for the application considered here, namely the solution of corrected HNC equations formed by including the third- and fourth-order bridge graphs in various ways. These calculations are similar to those carried out for the hard-sphere fluid by Samec (1971).

The organisation of the paper is as follows. In §2 the Abe–Meeron expansion is reviewed briefly and put into dimensionless Fourier-transformed form. The analytic reduction of the bridge graphs of order Λ^3 and Λ^4 in §3 is followed in §4 by their numerical evaluation. In §5 the modified HNC calculations are described and, finally, results and conclusions are given in §6.

2. The Abe–Meeron expansion

It is well known that all graphs in the usual Mayer expansion in powers of density diverge for the OCP due to the long range of the Coulomb potential. This difficulty is overcome by the Abe–Meeron resummation (Meeron 1958, Abe 1959, Hirt 1965) which yields expressions for the OCP binary correlation functions as sums of two-rooted irreducible graphs. In these each field point represents a factor ρ and there are two distinct bond functions: the Debye line

$$v(r) = -\frac{\beta(Ze)^2}{r} \exp\left(-\frac{r}{\lambda_D}\right),$$

no two of which may occur in series, and the Meeron line

$$w(r) = \exp(v(r)) - 1 - v(r).$$

A graph with two root points (1 and 2), n field points, l Debye lines joining pairs of points (i, j) and m Meeron lines joining pairs of points (p, q) represents the integral

$$I(r_{12}) = \sigma\rho^n \int \mathrm{d}^3 r_3 \ldots \int \mathrm{d}^3 r_{n+2} \prod_1^l v(r_{ij}) \prod_1^m w(r_{pq})$$

where σ is a combinatorial factor. Expressing this last equation in terms of the dimensionless length ξ and the functions

$$v(\xi) = -(\Lambda/\xi)\, \mathrm{e}^{-\xi} \tag{17}$$

$$w(\xi) = \exp(v(\xi)) - 1 - v(\xi) \tag{18}$$

we obtain

$$I(\xi_{12}) = \sigma(4\pi\Lambda)^{-n} \int \mathrm{d}^3 \xi_3 \ldots \int \mathrm{d}^3 \xi_{n+2} \prod_1^l v(\xi_{ij}) \prod_1^m w(\xi_{pq}). \tag{19}$$

The Fourier transform $\hat{w}(k)$ of $w(\xi)$ has been expressed as an infinite series in Λ and $\ln\Lambda$ (Del Rio and De Witt 1969, Furutani and Deutsch 1977, Guernsey 1978) from which

$$\hat{w}(k)=\frac{2\pi\Lambda^2}{k}\tan^{-1}(\tfrac{1}{2}k)+O(\Lambda^3\ln\Lambda).$$

As will be seen below, the third-order bridge graph contains no w bond and the fourth-order bridge graphs contain at most one. Thus, for the present purpose of an expansion in Λ, $w(\xi)$ may be replaced by

$$w_1(\xi)=\tfrac{1}{2}\Lambda^2 e^{-2\xi}/\xi^2.$$

It follows that, for the restricted set of bridge graphs considered, (19) simplifies to

$$I(\xi_{12})=\sigma(-1)^l(4\pi)^{-n}\Lambda^{l+2m-n}\int d^3\xi_3\ldots\int d^3\xi_{n+2}\prod_1^l\frac{e^{-\xi_{ij}}}{\xi_{ij}}\prod_1^m\frac{e^{-2\xi_{pq}}}{2\xi_{pq}^2}. \tag{20}$$

It is now possible, using (20), to enumerate all bridge graphs (irreducible two-rooted graphs which cannot be subdivided into two parts connected in series or in parallel) of orders Λ^3 and Λ^4. They are shown in figure 1 where the lines are Debye lines and $w_1(\xi)$ is represented as a two-bubble. Figure 1(a) is the single third-order bridge graph while the remainder are all of fourth order.

These graphs have been listed previously by Deutsch *et al* (1976), who did not, however, deal with the combinatorial factors σ shown for each graph in figure 1. The values of σ can be explained as follows. (i) For each graph there is the reciprocal of its

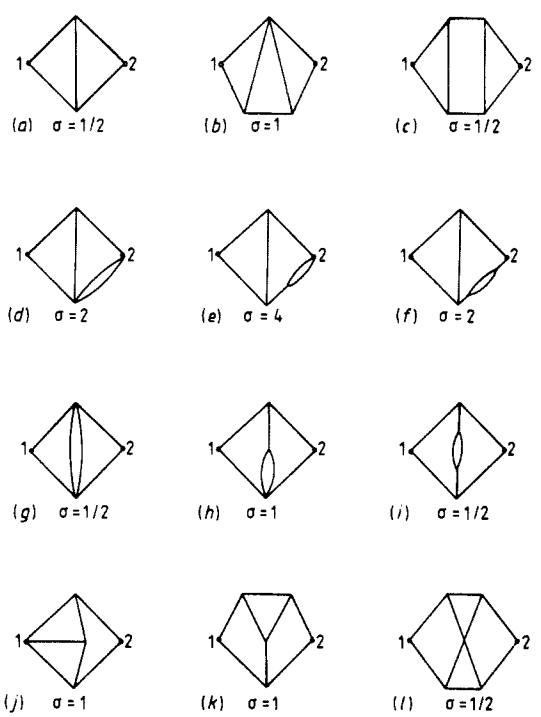

Figure 1. The bridge graphs of orders Λ^3 and Λ^4.

symmetry number (the number of permutations of field points leaving the graph invariant). (ii) Interchanging the root points 1 and 2 in graphs (*d*), (*e*), (*f*) and (*j*) yields distinct graphs, and so these graphs must have an extra factor two in σ. (iii) Reversing the order of the Debye line and two-bubble occurring in series in graph (*e*) generates two distinct graphs of identical value. Therefore (*e*) must have a further factor of two in σ.

Since the maximum number of field points in figure 1 is four, the corresponding integrals have (excluding a trivial azimuthal angle) maximum dimension eleven, which is rather high for numerical evaluation. Fortunately the situation is improved by Fourier transforming the graphs. This is achieved by substituting in (20) the relations

$$\frac{\exp(-\xi_{ij})}{\xi_{ij}} = \frac{1}{2\pi^2}\int \mathrm{d}^3k\, \exp[\mathrm{i}\boldsymbol{k}\cdot(\boldsymbol{\xi}_j-\boldsymbol{\xi}_i)]\frac{1}{1+k^2} \tag{21}$$

and

$$\frac{\exp(-2\xi_{pq})}{2\xi_{pq}^{\ 2}} = \frac{1}{2\pi^2}\int \mathrm{d}^3k\, \exp[\mathrm{i}\boldsymbol{k}\cdot(\boldsymbol{\xi}_q-\boldsymbol{\xi}_p)]\frac{\tan^{-1}(\frac{1}{2}\mathrm{k})}{2k} \tag{22}$$

followed by simplifying the resulting expression using

$$\delta(\boldsymbol{k}) = (2\pi)^{-3}\int \mathrm{d}^3\xi\, \exp(\mathrm{i}\boldsymbol{k}\cdot\boldsymbol{\xi}) \tag{23}$$

and

$$I(\xi_{12}) = (2\pi)^{-3}\int \mathrm{d}^3k\, \exp(\mathrm{i}\boldsymbol{k}\cdot\boldsymbol{\xi}_{12})\hat{I}(k). \tag{24}$$

$\hat{I}(k)$ may be represented graphically by adding to the graph for $I(\xi_{12})$ external lines with wavenumber k at 1 and 2 and then assigning wavenumbers to all internal lines in accordance with wavenumber conservation at each vertex. The evaluation of $\hat{I}(k)$ from its graph is carried out as follows.

(i) For each Debye line (labelled K) there is a factor $(1+K^2)^{-1}$.

(ii) For each two-bubble (labelled K) there is a factor $\frac{1}{2}\tan^{-1}(\frac{1}{2}K)/K$.

(iii) The resulting product is integrated over all internal wavenumbers.

(iv) The numerical factor multiplying this integral is

$$\sigma(2\pi)^3(-1)^l(2\pi^2)^{n-l-m}\Lambda^{l+2m-n}.$$

Figure 2 shows the Fourier-transformed graphs corresponding to the graphs of figure 1. In order to facilitate calculations the combinations

$$\hat{b}_{\mathrm{A}}(k) = \hat{b}_d(k)+\hat{b}_e(k)+\hat{b}_f(k) \tag{25}$$

and

$$\hat{b}_{\mathrm{S}}(k) = \hat{b}_g(k)+\hat{b}_h(k)+\hat{b}_i(k) \tag{26}$$

have been introduced, the broken lines representing the function $\frac{1}{2}Q^3\tan^{-1}(\frac{1}{2}Q)/(1+Q^2)^2$. There is some degree of flexibility in the assignment of internal wavenumbers, as illustrated by the two different choices for $\hat{b}_j(k)$; the reason for these will be made clear below. The maximum number of independent internal wavenumbers in figure 2 is three, and so the corresponding integrals now have maximum dimension eight (again excluding a trivial azimuthal angle).

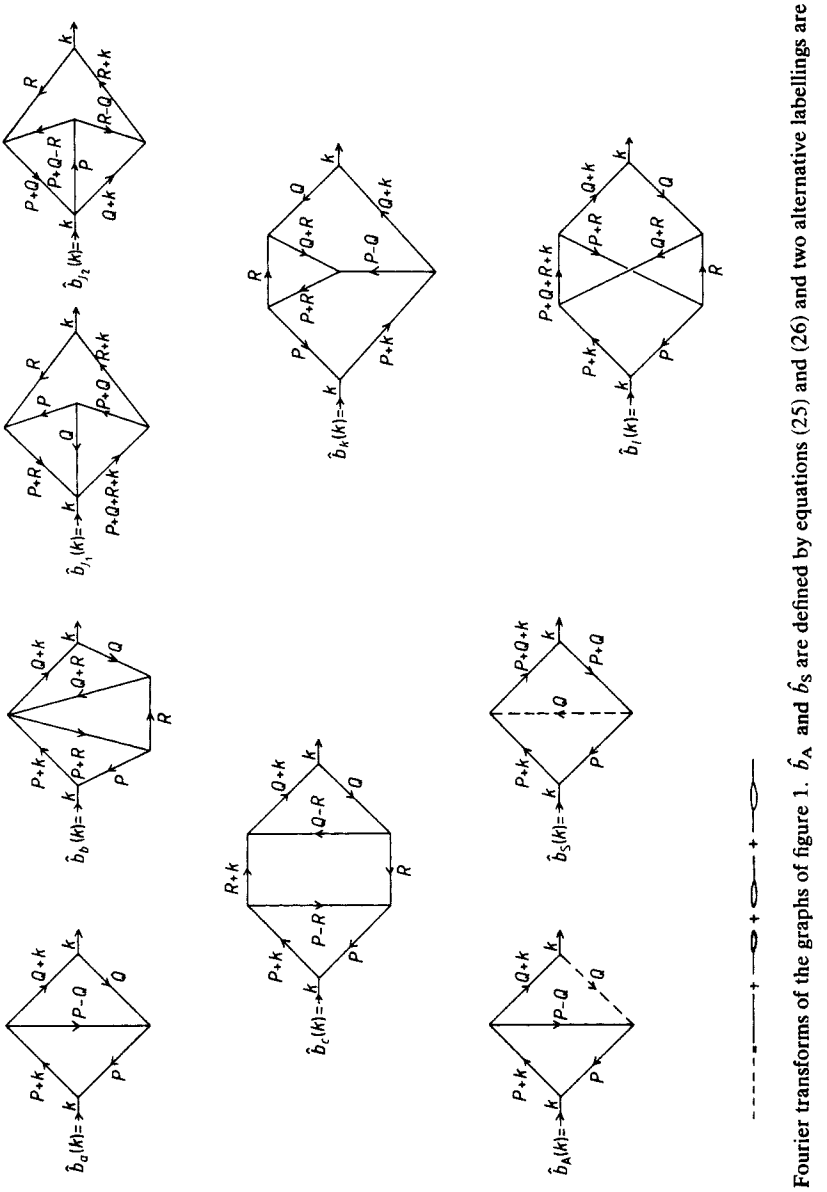

Figure 2. The Fourier transforms of the graphs of figure 1. $\hat{b}_A$ and $\hat{b}_S$ are defined by equations (25) and (26) and two alternative labellings are given for $\hat{b}_l$.

3. Analytic simplification of the bridge graph integrals

Further reduction of the dimensions of the integrals represented in figure 2 may be achieved by using the Goursat–Feynman relations which are described in the appendix. These methods were introduced in the context of the OCP by Mitchell and Ninham (1968) and were subsequently used by Deutsch *et al* (1976). The purpose of this section is to give the expressions for the bridge graph integrals which are used for their numerical evaluation in §4. Therefore the results are merely stated with minimal comment where appropriate.

For the first three graphs, all wavenumber integrations can be simplified using equations (A.3) and (A.6):

$$\hat{b}_a(k) = -\frac{\pi\Lambda^3}{2}\int_0^1 \frac{dx}{\theta_x}\int_0^1 \frac{dy}{\theta_y}\frac{1}{(x-y)^2k^2+(1+\theta_x+\theta_y)^2} \tag{27}$$

where

$$\theta_x^2 = x(1-x)k^2+1 \tag{28}$$

and

$$\theta_y^2 = y(1-y)k^2+1, \tag{29}$$

$$\hat{b}_b(k) = -\frac{\pi\Lambda^4}{2}\int_0^1 \frac{dx}{\theta_x}\int_0^1 \frac{dy}{\theta_y}\int_0^1 \frac{dz}{\delta}\frac{1}{(x-yz)^2k^2+(1+\theta_x+\delta)^2} \tag{30}$$

where

$$\delta^2 = z(1-z)y^2k^2+z(1+\theta_y)^2+(1-z) \tag{31}$$

and

$$\hat{b}_c(k) = \frac{\pi\Lambda^4}{4}\int_0^1 \frac{dx}{\theta_x}\int_0^1 \frac{dy}{\theta_y}\int_0^1 \frac{dz}{\theta_z}\int_0^1 \frac{dw}{\delta'}\frac{\theta_z+\delta'}{\{[x-z-(x-y)w]^2k^2+(\theta_z+\delta')^2\}^2} \tag{32}$$

where

$$\theta_z^2 = z(1-z)k^2+1 \tag{33}$$

and

$$\delta'^2 = w(1-w)(x-y)^2k^2+w(1+\theta_y)^2+(1-w)(1+\theta_x)^2. \tag{34}$$

For the remaining graphs it is impossible to treat the integration over Q using the results of the appendix after all other integrations have been so treated. These integrals over Q are evaluated in terms of spherical polar coordinates with polar axis along $\boldsymbol{k}$ and polar angle $\cos^{-1}t$ $(-1\leqslant t\leqslant 1)$. The integration over the azimuthal angle is always trivial, yielding a factor 2π, and the integration over t may sometimes be carried out analytically. In order to transform the radial integration to a finite interval the variable u defined by $Q = u/(1-u)$ $(0\leqslant u\leqslant 1)$ is introduced. The following results are obtained using equations (A.3), (A.5) and (A.6):

$$\hat{b}_A(k) = \frac{\Lambda^4}{k}\int_0^1 \frac{u^4\,du}{[u^2+(1-u)^2]^2}\tan^{-1}\left(\frac{\frac{1}{2}u}{1-u}\right)\int_0^1 \frac{dx}{\theta_x}\frac{\ln[(\varepsilon_2+\varepsilon_1)/(\varepsilon_2-\varepsilon_1)]}{(1-x)u^2+(2\theta_x+2-x)(1-u)^2}$$
$$(k\neq 0) \tag{35}$$

where

$$\varepsilon_1 = \alpha_1\alpha_4 - \alpha_2\alpha_3 \tag{36}$$

$$\varepsilon_2 = \alpha_2\alpha_4 - \alpha_1\alpha_3 \tag{37}$$

and

$$\alpha_1 = 2ku(1-u) \tag{38}$$

$$\alpha_2 = u^2 + (k^2+1)(1-u)^2 \tag{39}$$

$$\alpha_3 = 2kxu(1-u) \tag{40}$$

$$\alpha_4 = u^2 + [k^2x^2 + (1+\theta_x)^2](1-u)^2. \tag{41}$$

For the special case $k = 0$,

$$\hat{b}_A(0) = \frac{\Lambda^4}{2}\int_0^1 \frac{(1-u)u^5\,du}{(u^2-u+\frac{1}{2})^3(5u^2-8u+4)} \tan^{-1}\left(\frac{\frac{1}{2}u}{1-u}\right). \tag{42}$$

$$\hat{b}_S(k) = \Lambda^4\int_0^1 \frac{u^5 du}{[u^2+(1-u)^2]^2} \tan^{-1}\left(\frac{\frac{1}{2}u}{1-u}\right)\int_0^1\frac{dx}{\theta_x}\int_0^1\frac{dy}{\theta_y}\frac{B}{(u^2+A^2+B^2)^2-4A^2u^2} \tag{43}$$

where

$$A = k(x-y)(1-u) \tag{44}$$

and

$$B = (\theta_x+\theta_y)(1-u). \tag{45}$$

$$\hat{b}_{j_1}(k) = -\Lambda^4\int_0^1\frac{(1-u)^3u^2du}{u^2+(1-u)^2}\int_{-1}^1 dt\int_0^1\frac{dx}{\theta_x}\int_0^1\frac{dy}{\Theta'}\int_0^1\frac{dz}{\Delta} \times\frac{\Theta+\Theta'+\Delta}{[(z-x)^2k^2(1-u)^2+2(z-x)(z-y)ktu(1-u)+(z-y)^2u^2+(\Theta+\Theta'+\Delta)^2]^2} \tag{46}$$

where

$$\Theta = (1-u)\theta_x \tag{47}$$

$$\Theta'^2 = y(1-y)u^2+(1-u)^2 \tag{48}$$

and

$$\Delta^2 = z(1-z)[u^2+2ktu(1-u)+k^2(1-u)^2]+(1-u)^2. \tag{49}$$

$$\hat{b}_{j_2}(k) = -\Lambda^4\int_0^1(1-u)^3u^2\,du\int_{-1}^1\frac{dt}{\alpha_1t+\alpha_2}\int_0^1\frac{dx}{\theta_x}\int_0^1\frac{dy}{\Theta'}\int_0^1\frac{dz}{\Delta'} \times\frac{\Theta+\Delta'}{[x^2k^2(1-u)^2+2x(1-yz)ktu(1-u)+(1-yz)^2u^2+(\Theta+\Delta')^2]^2} \tag{50}$$

where

$$\Delta'^2 = z(1-z)y^2u^2+z(1-u+\Theta')^2+(1-z)(1-u)^2. \tag{51}$$

$$\hat{b}_k(k) = \Lambda^4\int_0^1\frac{(1-u)^5u^2\,du}{u^2+(1-u)^2}\int_{-1}^1\frac{dt}{\alpha_1t+\alpha_2}\int_0^1\frac{dx}{\theta_x}\int_0^1\frac{dy}{\Theta'}\int_0^1\frac{dz}{\Delta'} \times\frac{\Theta+\Delta'}{[x^2k^2(1-u)^2+2x(1-yz)ktu(1-u)+(1-yz)^2u^2+(\Theta+\Delta')^2]^2}. \tag{52}$$

$$\hat{b}_l(k) = \frac{\Lambda^4}{2}\int_0^1 \frac{(1-u)^5u^2\,du}{u^2+(1-u)^2}\int_{-1}^1 \frac{dt}{\alpha_1 t+\alpha_2}\int_0^1 \frac{dx}{\theta_x}\int_0^1 \frac{dy}{\Theta'}\int_0^1 \frac{dz}{\Delta} \times \frac{\Theta+\Theta'+\Delta}{[(z-x)^2k^2(1-u)^2+2(z-x)(z-y)ktu(1-u)+(z-y)^2u^2+(\Theta+\Theta'+\Delta)^2]^2}. \tag{53}$$

Clearly there are strong similarities between (46) and (53) and between (50) and (52); that is, $\hat{b}_l(k)$ may be cast in two different forms, one similar to $\hat{b}_k(k)$ and one similar to $\hat{b}_l(k)$. It is thus convenient to evaluate as a single entity the combination

$$\hat{b}_V(k) = \hat{b}_l(k) + \hat{b}_k(k) + \hat{b}_l(k). \tag{54}$$

It would be easy to perform the integration over t analytically in (50) and (52) but not in (46) and (53) (due to the t dependence of Δ). Therefore, since the combination $\hat{b}_V(k)$ is considered, none of these integrations over t is performed analytically.

4. Numerical evaluation of the bridge graphs

The single integral (42) for $\hat{b}_A(0)$ was evaluated using a compound Simpson's rule. Almost all of the multi-dimensional integrals required were evaluated using the Harwell subroutine QB01A which uses product formulae and allows different dimensions of the integration to be tackled by independent algorithms chosen from (1–16)-point Gaussian quadrature, Chebyshev integration and an adaptive Simpson's rule. Of these, the former is simplest and quickest but it is difficult to gauge its accuracy except by comparison with the latter pair, both of which can be assigned a fixed (relative) accuracy which QB01A seeks to achieve. In the Chebyshev case, however, the accuracy assigned is sometimes not achieved and the adaptive Simpson's rule uses a prohibitive amount of computer time for hard integrals of high dimension. Indeed, the present integration techniques are only just feasible for a five-dimensional integral (with a parameter) and for any higher-dimensional integral it would be necessary to use a Monte Carlo integration method.

Initially each of the functions $\hat{b}_a$, $\hat{b}_b$, $\hat{b}_c$, $\hat{b}_A$, $\hat{b}_S$ and $\hat{b}_V$ was evaluated for $0.0 \leq k \leq 10.0$ at intervals of 0.1. For $\hat{b}_a$, $\hat{b}_A$, $\hat{b}_b$ and $\hat{b}_S$ these evaluations were all achieved using the adaptive Simpson's rule for each dimension with accuracy 10^{-4}. The higher-dimensional integrals $\hat{b}_c$ and $\hat{b}_V$ were evaluated using 16-point Gaussian quadrature for each dimension and a few of the results were checked against more time-consuming Simpson's-rule calculations. The two sets of results were found to agree to at least two significant figures and so, in view of the lower order of magnitude of $\hat{b}_c$ and $\hat{b}_V$ compared with the other integrals of order Λ^4 (see figure 4), the values obtained for $\hat{b}_c$ and $\hat{b}_V$ using 16-point Gaussian quadrature were deemed satisfactory. In evaluating $\hat{b}_V$, a choice had to be made between the two alternative expressions (46) and (50) for $\hat{b}_l$. It was found, by comparison with the Simpson's-rule results, that, when $\hat{b}_l$ was calculated using 16-point Gaussian quadrature, (50) was more accurate for $k \leq 2.0$ while (46) was preferable for $k > 2.0$.

Figure 3 shows the third-order bridge graph

$$\hat{b}_3(k) = \hat{b}_a(k) \tag{55}$$

for $0.0 \leq k \leq 10.0$. For the same range of k, the individual fourth-order bridge graphs

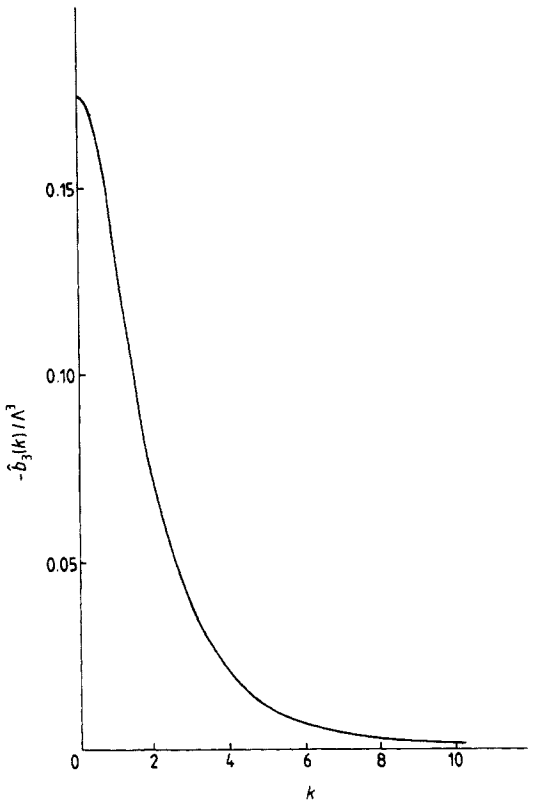

Figure 3. The Fourier-transformed bridge graph of order Λ^3.

are displayed together in figure 4 and their sum

$$\hat{b}_4(k) = \hat{b}_A(k) + \hat{b}_S(k) + \hat{b}_b(k) + \hat{b}_c(k) + \hat{b}_V(k) \tag{56}$$

is shown in figure 5. In addition, table 1 gives some numerical values for $\hat{b}_3(k)$ and $\hat{b}_4(k)$.

The input required for a modified HNC theory as outlined in §1 is some approximant to $b(\xi)$ rather than to $\hat{b}(k)$. In order to obtain $b_3(\xi)$ and $b_4(\xi)$ from $\hat{b}_3(k)$ and $\hat{b}_4(k)$ respectively the asymptotic behaviour of the latter functions as $k \to \infty$ must be determined. It is difficult to do this analytically and it is therefore necessary to rely on the results of numerical quadrature but, as will now be shown, analysis can give some indication of the functional form of $\hat{b}_3(k)$ and $\hat{b}_4(k)$ in the limit $k \to \infty$.

In considering $\hat{b}_3(k)$, given by (27), it is convenient to divide the square region of integration into parts:

(I) $\quad k^{-1} \leqslant x \leqslant 1-k^{-1} \qquad k^{-1} \leqslant y \leqslant 1-k^{-1}$

(II) $\quad k^{-1} \leqslant x \leqslant 1-k^{-1} \qquad 0 \leqslant y \leqslant k^{-1}.$

Due to the symmetry of the integrand in (27) under reflection in both diagonals of the integration region, there are three other subregions which give the same contribution to $\hat{b}_3(k)$ as (II). For $k \gg 1$ the following approximations are valid. In (I),

$$\theta_x^2 \sim k^2 x(1-x) \qquad \theta_y^2 \sim k^2 y(1-y),$$

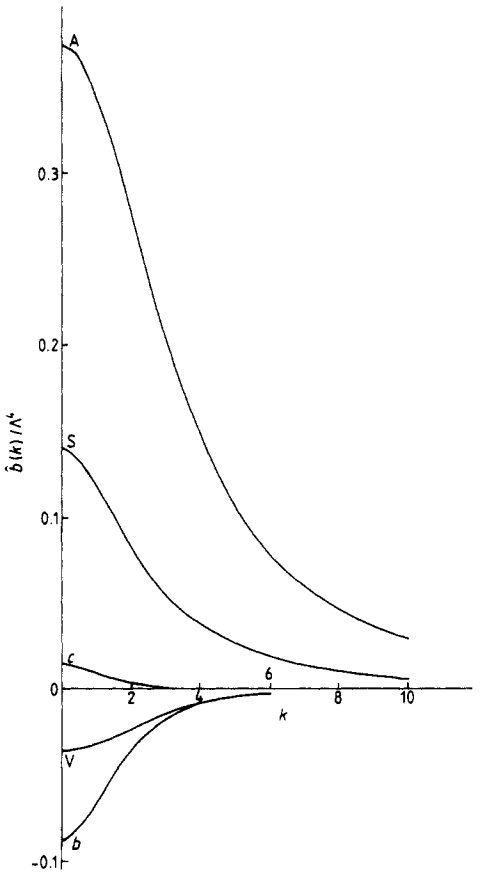

Figure 4. The individual Fourier-transformed bridge graphs of order Λ^4.

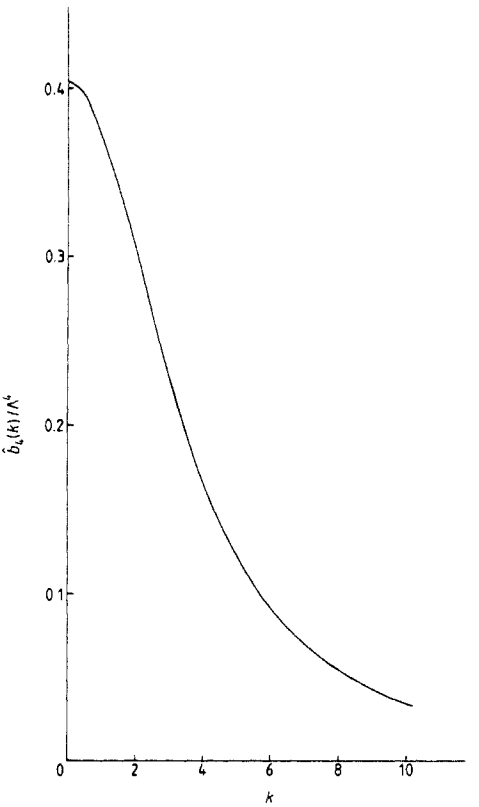

Figure 5. The total Fourier-transformed bridge function of order Λ^4.

leading to a contribution to $\hat{b}_3(k)$ of order $\ln k/k^4$. In (II)

$$\theta_x^2 \sim k^2 x(1-x) \qquad x-y \sim x \qquad 1+\theta_x+\theta_y \sim \theta_x,$$

yielding a contribution of order $k^{-7/2}$ to $\hat{b}_3(k)$. It is difficult to approximate the integrand of (27) close to the points (0,0) and (1,1) in the limit $k \to \infty$ and this prevents a complete analytic estimation of $\hat{b}_3(k)$ in this limit.

It is important to notice, however, that, for large k, the dominant contribution to (27) comes from a thin strip around the edge of the square integration area. Thus, although the integrand is finite-valued everywhere for all k, it has a very sharply peaked behaviour near the boundary of the integration region when k is large. This almost singular behaviour stems from the appearance of θ_x^{-1} (and θ_y^{-1}) in the integrand. Since θ_x^{-1} is also present in all of the other integrals, they may be expected to have a similar, almost singular, behaviour for large k. It may therefore be anticipated that Gaussian quadrature will not give reliable results for any of these integrals at large k. This situation does not matter for the two- and three-dimensional integrals which may (as at low k) be evaluated using Simpson's rule, albeit with a reduced relative accuracy (10^{-3} for $k \geq 50$). For $\hat{b}_c(k)$ and $\hat{b}_V(k)$, where 16-point Gaussian quadrature was used at low

Table 1. Fourier-transformed bridge graphs.

k	$-\Lambda^{-3}\hat{b}_3(k)$	$\Lambda^{-4}\hat{b}_4(k)$
0.0	1.745×10^{-1}	4.039×10^{-1}
0.1	1.740×10^{-1}	4.036×10^{-1}
0.2	1.725×10^{-1}	4.026×10^{-1}
0.4	1.666×10^{-1}	3.987×10^{-1}
0.6	1.575×10^{-1}	3.923×10^{-1}
0.8	1.461×10^{-1}	3.838×10^{-1}
1.0	1.333×10^{-1}	3.733×10^{-1}
1.2	1.201×10^{-1}	3.612×10^{-1}
1.4	1.071×10^{-1}	3.477×10^{-1}
1.6	9.478×10^{-2}	3.333×10^{-1}
1.8	8.344×10^{-2}	3.182×10^{-1}
2.0	7.321×10^{-2}	3.027×10^{-1}
2.2	6.411×10^{-2}	2.870×10^{-1}
2.4	5.611×10^{-2}	2.715×10^{-1}
2.6	4.912×10^{-2}	2.563×10^{-1}
2.8	4.304×10^{-2}	2.415×10^{-1}
3.0	3.777×10^{-2}	2.274×10^{-1}
3.2	3.321×10^{-2}	2.137×10^{-1}
3.4	2.926×10^{-2}	2.008×10^{-1}
3.6	2.584×10^{-2}	1.887×10^{-1}
3.8	2.288×10^{-2}	1.772×10^{-1}
4.0	2.032×10^{-2}	1.665×10^{-1}
4.5	1.526×10^{-2}	1.425×10^{-1}
5.0	1.164×10^{-2}	1.223×10^{-1}
5.5	9.016×10^{-3}	1.054×10^{-1}
6.0	7.082×10^{-3}	9.130×10^{-2}
7.0	4.539×10^{-3}	6.946×10^{-2}
8.0	3.040×10^{-3}	5.386×10^{-2}
9.0	2.112×10^{-3}	4.251×10^{-2}
10.0	1.513×10^{-3}	3.410×10^{-2}

k, however, a general-purpose 10-point quadrature formula (Harris and Evans 1977) which can cope with integrable end-point singularities was used at large k. This formula was found to give results for $\hat{b}_a(k)$ in satisfactory agreement with those obtained using Simpson's rule.

The above analysis of $\hat{b}_3(k)$ suggests the asymptotic form

$$\hat{b}_3(k)=\frac{A}{k^{7/2}}+\frac{B\ln k}{k^4}+\frac{C}{k^4} \qquad k\to\infty. \tag{57}$$

$\hat{b}_3(k)$ was evaluated for several large values of k (in the range $20\leqslant k\leqslant 200$) using the adaptive Simpson's rule of QB01A. A least-squares fit of these values assuming the functional form (57) leads to the approximate result

$$\Lambda^{-3}\hat{b}_3(k)=-0.03350\,k^{-7/2}-12.53\,k^{-4}\ln k+13.91\,k^{-4} \qquad (k\geqslant 20), \tag{58}$$

which agrees with the calculated values of $\hat{b}_3(k)$ to within the relative accuracy set by QB01A.

The type of analysis of $\hat{b}_3(k)$ which led to (57) is not feasible for $\hat{b}_4(k)$ but it is clear that $b_a(\xi=0)$ represents a divergent integral. This divergence is not cancelled in order Λ^4 and it may therefore be concluded that $b_4(\xi=0)$ is also divergent. It follows that

$\hat{b}_4(k)$ falls off less rapidly than k^{-3} as $k \to \infty$, and that the major contribution to $\hat{b}_4(k)$ in this limit comes from $\hat{b}_A(k)$ (which includes $\hat{b}_d(k)$). All of the fourth-order bridge graphs were evaluated for several large values of k (in the range $10 \leq k \leq 100$) using the general-purpose integration formula of Harris and Evans (1977) mentioned above whenever it was impossible or unnecessary to use either Simpson's rule or Chebyshev integration. $\hat{b}_4(k)$ was approximated by various three-parameter functions (all consistent with its long range) and the best least-squares fit found was

$$\Lambda^{-4}\hat{b}_4(k) = -2.176\,k^{-5/2} + 33.69\,k^{-3}\ln k - 36.60k^{-3} \qquad (k \geq 10). \tag{59}$$

This fit is almost, but not quite, as accurate as (58). It must be regarded with suspicion for *very* large k since it then becomes negative whereas the true function $\hat{b}_4(k)$ is expected to remain positive for all k.

The numerical results for $\hat{b}_3(k)$ and $\hat{b}_4(k)$ together with the asymptotic expressions (58) and (59) permit $b_3(\xi)$ and $b_4(\xi)$ to be calculated by inverse Fourier transformation. The results for small ξ are shown in figures 6 and 7 and table 2. In the numerical Fourier transformation, the discontinuity at the cut-off point leads to spurious oscillations which become important at large ξ. The results at high ξ therefore had to be obtained by extrapolation from the intermediate ξ region using least-squares fits. The asymptotic

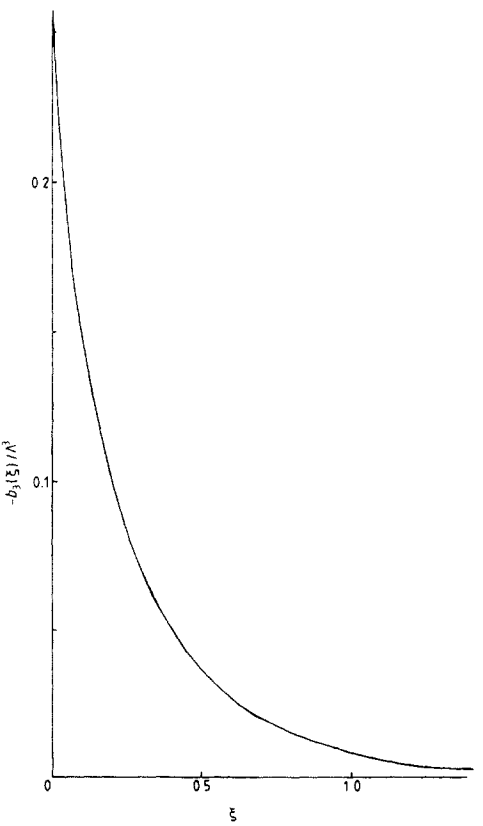

Figure 6. The configuration space bridge graph of order Λ^3.

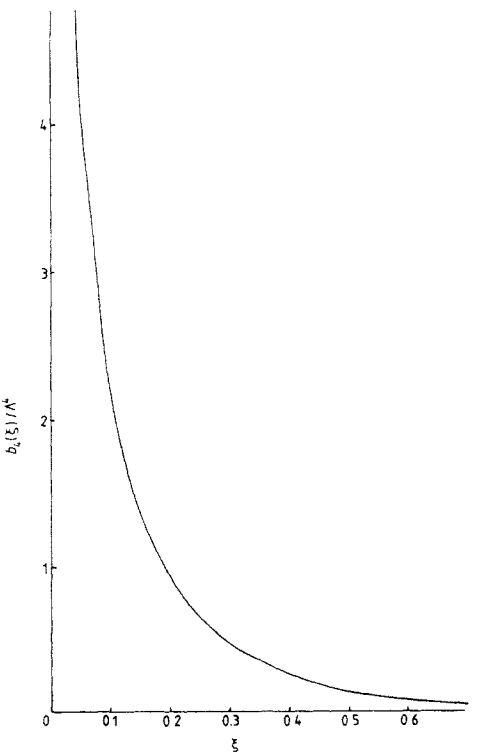

Figure 7. The contribution of order Λ^4 to the configuration space bridge function.

Table 2. Configuration space bridge graphs.

ξ	$-\Lambda^{-3}b_3(\xi)$	$\Lambda^{-4}b_4(\xi)$
0.00	2.569×10^{-1}	∞
0.02	2.192×10^{-1}	7.884×10^{0}
0.04	1.953×10^{-1}	5.023×10^{0}
0.06	1.763×10^{-1}	3.646×10^{0}
0.08	1.604×10^{-1}	2.809×10^{0}
0.10	1.467×10^{-1}	2.240×10^{0}
0.12	1.347×10^{-1}	1.829×10^{0}
0.14	1.241×10^{-1}	1.518×10^{0}
0.16	1.147×10^{-1}	1.276×10^{0}
0.18	1.062×10^{-1}	1.083×10^{0}
0.20	9.846×10^{-2}	9.271×10^{-1}
0.22	9.147×10^{-2}	7.988×10^{-1}
0.24	8.510×10^{-2}	6.922×10^{-1}
0.26	7.927×10^{-2}	6.027×10^{-1}
0.28	7.392×10^{-2}	5.270×10^{-1}
0.30	6.901×10^{-2}	4.626×10^{-1}
0.35	5.833×10^{-2}	3.385×10^{-1}
0.40	4.954×10^{-2}	2.518×10^{-1}
0.45	4.224×10^{-2}	1.896×10^{-1}
0.50	3.614×10^{-2}	1.443×10^{-1}
0.55	3.100×10^{-2}	1.107×10^{-1}
0.60	2.667×10^{-2}	8.555×10^{-2}
0.70	1.986×10^{-2}	5.188×10^{-2}
0.80	1.489×10^{-2}	3.197×10^{-2}
0.90	1.123×10^{-2}	1.995×10^{-2}
1.00	8.516×10^{-3}	1.258×10^{-2}
1.10	6.484×10^{-3}	8.001×10^{-3}
1.20	4.955×10^{-3}	5.112×10^{-3}
1.40	2.922×10^{-3}	2.086×10^{-3}
1.60	1.741×10^{-3}	8.578×10^{-4}

forms found in this way are

$$\Lambda^{-3}b_3(\xi) = -0.03696\,\frac{e^{-2\xi}}{\xi} - 0.1257\,\frac{e^{-2\xi}}{\xi^2} + 0.2238\,\frac{e^{-3\xi}}{\xi} \qquad (\xi \geqslant 2.5) \tag{60}$$

and

$$\Lambda^{-4}b_4(\xi) = 1.017\,e^{-5\xi} + 11.25\,\frac{e^{-5\xi}}{\xi} - 14.18\,\frac{e^{-5\xi}}{\xi^2} \qquad (\xi \geqslant 2.0). \tag{61}$$

The approximate formulae (60) and (61) are not nearly as reliable as (58) and (59), but this is not expected to be crucial to the modified HNC results below since the functions $b_3(\xi)$ and $b_4(\xi)$ are both very short ranged.

5. Modified HNC approximations

Letting

$$F(\xi) = -\Lambda^{-3}b_3(\xi) \tag{62}$$

and

$$G(\xi) = \Lambda^{-4} b_4(\xi) \tag{63}$$

the most obvious approximations to make for $b(\xi)$ are

$$b(\xi) = -\Lambda^3 F(\xi) \tag{64}$$

and

$$b(\xi) = -\Lambda^3 F(\xi) + \Lambda^4 G(\xi). \tag{65}$$

Both (64) and (65) may be expected to yield satisfactory modified HNC results in the weak-coupling regime $\Gamma \leqslant 0.7$ ($\Lambda \leqslant 1$). A 'generalised Padé' approximant is also considered in an attempt to extend the range of validity of the modified HNC results. This approximant has the form

$$b(\xi) = \frac{-\Lambda^3 F(\xi)}{[1 + (\Lambda/\omega)(G(\xi)/F(\xi))]^{\omega}}$$

which reproduces the correct $\Lambda \to 0$ limiting behaviour for arbitrary (real) ω. In order to obtain the expected strong-coupling behaviour ($b(\xi) \propto \Gamma \propto \Lambda^{2/3}$, $\Lambda \to \infty$) ω must be chosen as $\frac{7}{3}$, yielding

$$b(\xi) = \frac{-\Lambda^3 F(\xi)}{[1 + \frac{3}{7}\Lambda(G(\xi)/F(\xi))]^{7/3}}. \tag{66}$$

Equation (66) seems to represent the best hope for an approximation based on the above integrals which may remain valid beyond the weak-coupling regime.

All of the modified HNC theories considered here can be obtained by replacing equation (6) in the HNC approximation by

$$g(\xi) = \exp[-(\Lambda/\xi) + h(\xi) - c(\xi) + b(\xi)] \tag{67}$$

with $b(\xi)$ given by (64), (65) and (66) respectively. These theories have been solved numerically using a suitably modified form of the Ng (1974) iteration procedure (expressed in terms of Λ and ξ rather than Γ and x); the number of iterations required for convergence was about the same as for the usual HNC scheme.

The accuracy of the iteration procedure was checked by seeing that variation of the number and spacing of discrete mesh points for ξ and k did not significantly affect the results. A simpler criterion for accuracy was found to be agreement between the values of βu^{ex} calculated from (9*a*) and (9*b*). It had originally been felt that the Cooper (1973) solution of the HNC approximation might be a more suitable basis for the present calculations than the Ng method since the former is explicitly based on the Abe–Meeron expansion. It was found, however, that although the Cooper method gives accurate values for $h(\xi)$ it does not do so for $\hat{h}(k)$. Equations (9*a*) and (9*b*) are therefore not in agreement for the Cooper iteration scheme with only (9*a*) yielding an accurate value for βu^{ex}.

Modified HNC calculations were carried out for $\Gamma \leqslant 10$ though it should be remembered that the regime of interest in connection with inertial confinement plasmas is $\Gamma \leqslant 1$. The three different approximations (64), (65) and (66) were each used in turn but (65) gave no solutions for $\Gamma \geqslant 1$ where the bridge graphs of order Λ^4 dominate those of order Λ^3 for small ξ, leading to divergence of $g(\xi)$ as $\xi \to 0$.

6. Results and conclusions

The results obtained for the radial distribution function $g(\xi)$ and the (static) structure factor

$$S(k) = 1 + (4\pi\Lambda)^{-1}\hat{h}(k) \tag{68}$$

using the usual HNC approximation and the modified approximations with (64) and (66) are shown for $\Gamma = 1$ and $\Gamma = 10$ in tables 3–6. The three sets of results are remarkably similar to one another. The two major deficiencies of the HNC results for $g(\xi)$ are (Cooper 1973) that oscillations at large ξ have too small an amplitude and that $g(\xi)$ increases from zero too rapidly at small ξ. Table 5 shows that both of these aspects are improved by the modified approximations but the former only very slightly so. Table 6 shows that the amplitude of oscillations in $S(k)$ is also slightly increased in the modified approximations.

In table 7 are displayed the excess internal energies of the OCP as found by the various approximate theories using (9), together with the MC results of Slattery *et al*

Table 3. The OCP radial distribution function at $\Gamma = 1$.

	$g(\xi)$		
ξ	HNC	Equation (64)	Equation (66)
0.2	0.000	0.000	0.000
0.4	0.034	0.026	0.033
0.5	0.079	0.066	0.079
0.6	0.140	0.123	0.139
0.7	0.209	0.190	0.208
0.8	0.281	0.263	0.280
0.9	0.353	0.336	0.351
1.0	0.422	0.408	0.420
1.1	0.486	0.474	0.484
1.2	0.546	0.536	0.543
1.3	0.600	0.593	0.598
1.4	0.648	0.644	0.646
1.5	0.692	0.689	0.690
1.6	0.731	0.729	0.729
1.7	0.765	0.765	0.764
1.8	0.795	0.796	0.795
1.9	0.822	0.823	0.821
2.0	0.845	0.847	0.845
2.2	0.884	0.885	0.884
2.4	0.913	0.914	0.913
2.6	0.935	0.936	0.935
2.8	0.951	0.952	0.952
3.0	0.964	0.964	0.964
3.5	0.983	0.983	0.983
4.0	0.992	0.992	0.992
4.5	0.996	0.996	0.996
5.0	0.998	0.998	0.998
5.5	0.999	0.999	0.999
6.0	1.000	1.000	1.000

Table 4. The OCP structure factor at $\Gamma = 1$.

	$S(k)$		
k	HNC	Equation (64)	Equation (66)
0.0	0.000	0.000	0.000
0.1	0.010	0.010	0.010
0.2	0.039	0.039	0.039
0.3	0.085	0.084	0.084
0.4	0.143	0.143	0.143
0.5	0.211	0.210	0.211
0.6	0.285	0.283	0.284
0.7	0.359	0.357	0.358
0.8	0.433	0.429	0.432
0.9	0.502	0.498	0.501
1.0	0.567	0.562	0.565
1.2	0.678	0.673	0.677
1.4	0.765	0.760	0.764
1.6	0.831	0.825	0.830
1.8	0.878	0.874	0.878
2.0	0.913	0.910	0.913
2.2	0.938	0.936	0.938
2.4	0.956	0.954	0.956
2.6	0.968	0.967	0.969
2.8	0.978	0.977	0.978
3.0	0.984	0.984	0.984
3.5	0.993	0.994	0.993
4.0	0.997	0.998	0.997
4.5	0.999	1.000	0.999
5.0	1.000	1.000	1.000
6.0	1.000	1.001	1.000

(1980) obtained from the least-squares fit

$$\beta u^{ex} = -0.89752\Gamma + 0.94544\Gamma^{1/4} - 0.80049 + 0.17954\Gamma^{-1/4} \tag{69}$$

for $\Gamma \geqslant 1$ and from their tabulated results for $\Gamma < 1$. For $\Gamma \leqslant 0.4$ the HNC results seem to be accurate since none of the bridge graphs added in the modified theories affects them appreciably. The close agreement among all the theoretical results, excluding those based on the questionable (65), for $\Gamma \leqslant 0.7$ suggests that the theories may be more reliable than MC simulations in this range of the coupling parameter. Thus these HNC and modified HNC results partially fill a gap in accurate results for βu^{ex} between $\Gamma = 0.1$, below which the Debye–Hückel theory is satisfactory, and $\Gamma = 1$, above which (69) is believed to be exact. If the MC data are indeed exact for $\Gamma \geqslant 1$ then table 7 shows that the modified HNC theories based on (64) and (66) improve on the usual HNC values of βu^{ex}, at least for $1 \leqslant \Gamma \leqslant 10$. For $\Gamma = 10$, however, this improvement is only slight.

Table 8 shows the inverse compressibility of the OCP as found in the various approximations through equation (11). The final column of MC results is calculated from the MC energy results using (12). It is clear from this table that using (66) for $b(\xi)$ yields an improvement in compressibility values compared with the HNC results. However, for $\Gamma \geqslant 2$, which coincides approximately with the onset of short-range order and of negative compressibility, the small improvement in compressibility values brought about by using (66) still leaves the results very inaccurate.

Table 5. The OCP radial distribution function at $\Gamma = 10$.

	$g(\xi)$		
ξ	HNC	Equation (64)	Equation (66)
2.8	0.000	0.000	0.000
3.2	0.001	0.000	0.000
3.6	0.007	0.001	0.001
4.0	0.024	0.010	0.011
4.4	0.063	0.046	0.046
4.8	0.132	0.117	0.117
5.2	0.232	0.224	0.224
5.6	0.358	0.356	0.356
6.0	0.499	0.502	0.502
6.4	0.641	0.647	0.647
6.8	0.773	0.780	0.780
7.2	0.885	0.892	0.892
7.6	0.973	0.979	0.979
8.0	1.036	1.041	1.041
8.4	1.077	1.080	1.080
8.8	1.098	1.101	1.101
9.2	1.105	1.106	1.106
9.6	1.101	1.101	1.101
10.0	1.090	1.090	1.090
11.0	1.051	1.050	1.050
12.0	1.016	1.014	1.014
13.0	0.995	0.994	0.994
14.0	0.987	0.987	0.987
16.0	0.993	0.994	0.994
18.0	1.001	1.001	1.001
20.0	1.002	1.002	1.002
22.0	1.000	1.000	1.000

In conclusion, it has turned out as expected that, overall, the best of the modified HNC theories above is provided by equation (66) although results based on (66) are not uniformly superior to those based on (64). For $\Gamma \leqslant 10$, the HNC values of $g(\xi)$ and especially βu^{ex} are already quite accurate. Using (66) or (64) for $b(\xi)$ does not change the values very much but does cause marginal improvement. In the range $\Gamma \leqslant 0.7$, the close agreement of HNC results for βu^{ex} with those obtained using (64) and (66) enhances confidence in all three sets of results. Finally, (66) leads to a significant improvement in compressibility values for $\Gamma \leqslant 2$. Since the corresponding excess internal energies are known to be accurate, this implies an improvement in thermodynamic consistency, lack of which is the major shortcoming of the unmodified HNC theory in this range of coupling strengths.

Acknowledgments

I am grateful to Professor E W Laing for helpful discussions. During part of this research I was supported by a studentship from the Carnegie Trust for the Universities of Scotland.

Table 6. The OCP structure factor at $\Gamma = 10$.

	$S(k)$		
k	HNC	Equation (64)	Equation (66)
0.00	0.000	0.000	0.000
0.10	0.010	0.010	0.010
0.20	0.046	0.046	0.046
0.30	0.120	0.120	0.120
0.40	0.259	0.258	0.258
0.44	0.339	0.337	0.337
0.48	0.434	0.430	0.430
0.52	0.541	0.537	0.537
0.56	0.657	0.651	0.651
0.60	0.773	0.767	0.767
0.64	0.880	0.875	0.875
0.68	0.970	0.966	0.966
0.72	1.038	1.035	1.035
0.76	1.081	1.080	1.080
0.80	1.104	1.104	1.104
0.84	1.109	1.111	1.111
0.88	1.104	1.107	1.106
0.92	1.091	1.094	1.094
0.96	1.075	1.078	1.078
1.00	1.058	1.062	1.061
1.10	1.021	1.024	1.024
1.20	0.999	1.000	1.000
1.40	0.988	0.988	0.988
1.60	0.995	0.994	0.994
1.80	1.000	1.000	1.000
2.00	1.001	1.001	1.001
2.50	1.000	1.000	1.000

Table 7. Excess internal energy of the OCP.

	$-\beta u^{ex}$				
Γ	HNC	Equation (64)	Equation (65)	Equation (66)	MC
0.1	0.02568	0.02568	0.02568	0.02568	—
0.2	0.06848	0.06849	0.06848	0.06849	—
0.3	0.1195	0.1196	0.1195	0.1195	0.1225
0.4	0.1759	0.1761	0.1757	0.1759	0.1784
0.5	0.2360	0.2364	0.2356	0.2362	0.2383
0.6	0.2991	0.2999	0.2979	0.2993	0.3018
0.7	0.3644	0.3657	0.3619	0.3647	0.3668
0.8	0.4317	0.4336	0.4266	0.4321	0.4337
0.9	0.5004	0.5032	0.4900	0.5010	0.5035
1.0	0.5705	0.5743	—	0.5712	0.5730
2.0	1.3153	1.3334	—	1.3193	1.3202
4.0	2.9109	2.9434	—	2.9275	2.9266
6.0	4.5621	4.5912	—	4.5858	4.5912
10.0	7.9354	7.9494	—	7.9492	7.9935

Table 8. Inverse compressibility of the OCP.

	$\beta(\partial p/\partial\rho)_\beta$				
Γ	HNC	Equation (64)	Equation (65)	Equation (66)	MC
0.1	0.9873	0.9873	0.9873	0.9873	—
0.2	0.9663	0.9667	0.9666	0.9666	—
0.3	0.9414	0.9424	0.9419	0.9421	—
0.4	0.9138	0.9161	0.9144	0.9152	0.9148
0.5	0.8842	0.8884	0.8845	0.8866	0.8863
0.6	0.8531	0.8599	0.8521	0.8566	0.8566
0.7	0.8207	0.8308	0.8173	0.8256	0.8264
0.8	0.7873	0.8012	0.7798	0.7937	0.7947
0.9	0.7528	0.7713	0.7384	0.7610	0.7625
1.0	0.7176	0.7411	—	0.7277	0.7305
2.0	0.3332	0.4170	—	0.3691	0.3875
4.0	−0.5307	−0.3938	—	−0.4389	−0.3408
6.0	−1.460	−1.345	—	−1.359	−1.091
10.0	−3.423	−3.373	—	−3.374	−2.618

Appendix. Derivation of relations used in § 3

For $a>0$ and $b>0$,

$$\frac{1}{ab}=\int_0^1 \frac{\mathrm{d}x}{[ax+b(1-x)]^2}. \tag{A.1}$$

Also, for $A>0$ and $B>0$,

$$\int \frac{\mathrm{d}^3Q}{(Q^2+A^2)[(\boldsymbol{Q}+\boldsymbol{k})^2+B^2]^2}=\frac{\pi^2}{B}\frac{1}{k^2+(A+B)^2}. \tag{A.2}$$

Applying (A.1) and then (A.2) gives

$$\int \frac{\mathrm{d}^3Q}{(Q^2+A^2)[(\boldsymbol{Q}+\boldsymbol{k}_1)^2+B_1^2][(\boldsymbol{Q}+\boldsymbol{k}_2)^2+B_2^2]}=\pi^2\int_0^1\frac{\mathrm{d}x}{\theta}\frac{1}{(\boldsymbol{k}_2-x\boldsymbol{k}_1)^2+(B_2+\theta)^2} \tag{A.3}$$

where

$$\theta^2=x(1-x)k_1^2+xB_1^2+(1-x)A^2. \tag{A.4}$$

Differentiating (A.3) with respect to B_2 results in

$$\int \frac{\mathrm{d}^3Q}{(Q^2+A^2)[(\boldsymbol{Q}+\boldsymbol{k}_1)^2+B_1^2][(\boldsymbol{Q}+\boldsymbol{k}_2)^2+B_2^2]^2}=\frac{\pi^2}{B_2}\int_0^1\frac{\mathrm{d}x}{\theta}\frac{B_2+\theta}{[(\boldsymbol{k}_2-x\boldsymbol{k}_1)^2+(B_2+\theta)^2]^2}. \tag{A.5}$$

Finally, using (A.1) and then (A.5) yields

$$\int \frac{\mathrm{d}^3Q}{(Q^2+A^2)[(\boldsymbol{Q}+\boldsymbol{k}_1)^2+B_1^2][(\boldsymbol{Q}+\boldsymbol{k}_2)^2+B_2^2][(\boldsymbol{Q}+\boldsymbol{k}_3)^2+B_3^2]}$$
$$=\pi^2\int_0^1\frac{\mathrm{d}x}{\theta}\int_0^1\frac{\mathrm{d}y}{\theta'}\frac{\theta+\theta'}{\{[x\boldsymbol{k}_1-(1-y)\boldsymbol{k}_2-y\boldsymbol{k}_3]^2+(\theta+\theta')^2\}^2} \tag{A.6}$$

where

$$\theta'^2 = y(1-y)(\boldsymbol{k}_3-\boldsymbol{k}_2)^2 + yB_3^2 + (1-y)B_2^2. \tag{A.7}$$

References

Abe R 1959 *Prog. Theor. Phys.* **22** 213
Baus M and Hansen J P 1980 *Phys. Rep.* **59** 1
Brush S G, Sahlin H L and Teller E 1966 *J. Chem. Phys.* **45** 2102
Cooper M S 1973 *Phys. Rev.* A **7** 1
Del Rio F and De Witt H E 1969 *Phys. Fluids* **12** 791
Deutsch C, Furutani Y and Gombert M M 1976 *Phys. Rev.* A **13** 2244
—— 1979 *J. Phys. A: Math. Gen.* **12** L317
—— 1981 *Phys. Rep.* **69** 85
De Witt H E 1976 *Phys. Rev.* A **14** 1290
Furutani Y and Deutsch C 1977 *J. Math. Phys.* **18** 292
Furutani Y, Deutsch C and Oda Y 1981 *J. Physique Lett.* **42** L285
Galam S and Hansen J P 1976 *Phys. Rev.* A **14** 816
Guernsey R L 1978 *Phys. Fluids* **21** 2162
Hansen J P 1973 *Phys. Rev.* A **8** 3096
Harris C G and Evans W A B 1977 *Int. J. Comput. Math.* **6** 219
Hirt C W 1965 *Phys. Fluids* **8** 693
—— 1967 *Phys. Fluids* **10** 565
Jancovici B 1977 *J. Stat. Phys.* **17** 357
Ladø F 1973 *Phys. Rev.* A **8** 2548
Lavaud M 1977 *Phys. Lett.* **63A** 76
MacGowan D 1981 *Phys. Lett.* **84A** 427
Meeron E 1958 *J. Chem. Phys.* **28** 630
Mitchell D J and Ninham B W 1968 *Phys. Rev.* **174** 280
Ng K C 1974 *J. Chem. Phys.* **61** 2680
Rosenfeld Y and Ashcroft N W 1979 *Phys. Rev.* A **20** 1208
Samec A 1971 *J. Chem. Phys.* **54** 2178
Slattery W L, Doolen G D and De Witt H E 1980 *Phys. Rev.* A **21** 2087
Springer J F, Pokrant M A and Stevens F A Jr 1973 *J. Chem. Phys.* **58** 4863